

# Effect of Ring Exchange on Orbital Antiferromagnet

C. H. Chung, Hae-Young Kee and Yong Baek Kim

*Department of Physics, University of Toronto, Ontario, Canada M5S 1A7*

(February 1, 2008)

We study the effect of four-particle ring exchange process on orbital antiferromagnetic state that occurs in some correlated electron systems in two dimensions. The primary question is whether the ring exchange process enhances or suppresses the orbital antiferromagnetic ordering. Using the fact that the orbital antiferromagnetic state arises in the large- $N$  limit of the  $SU(N)$  generalization of the  $t$ - $J$  model, we consider the large- $N$  limit of the  $t$ - $J$ - $K$  model where  $K$  represents the four-particle ring exchange term. The phase diagrams in the large- $N$  mean field theory are obtained for the half-filling and finite hole concentrations at zero temperature. It is found that the ring exchange in general favors dimerized states or the inhomogeneous orbital antiferromagnetic state, and suppresses the homogeneous orbital antiferromagnetic state. We compare our results with other related models of strongly correlated systems with ring exchange processes.

PACS numbers: 71.10.Hf, 71.10.Fd, 71.30.+h, 75.10.Jm

## I. INTRODUCTION

Ring exchange interactions are often present in strongly correlated many-particle systems. In the Hubbard model of electrons with on-site repulsive interaction  $U$ , the large  $U$  limit leads to an antiferromagnetic exchange interaction  $J \sim t^2/U$  between electrons at nearby sites where  $t$  is the hopping amplitude of electrons. It was shown that the next leading order term in the effective Hamiltonian is the four-particle ring exchange interaction with the strength  $K \sim t^3/U^2$  [1]. The multi-particle ring exchange interactions have been studied extensively in solid  $^3\text{He}$  [2]. It was also suggested that the ring exchange interactions may play an important role in understanding the ‘metal-insulator’ transition in low density two-dimensional electron systems [3]. More recently, ring exchange models have been revisited in the context of the occurrence of novel quantum ground states in strongly correlated electrons, bosons, and spin systems [4,5,6,7]. In particular the possibility of fractionalized phases where the elementary excitations carry fractions of quantum numbers of electrons/spins has been discussed [4,5]. It was also suggested that in some soft-core boson models with ring exchange interactions, there may exist a novel phase which is neither a superfluid nor a conventional insulator; the low energy excitations in this phase are described by a continuous set of wavevectors with zero energy, which may be called a Bose ‘surface’ in analogy to the familiar Fermi surface of electrons [6]. On the other hand, a quantum Monte Carlo study of a quantum XY model with a ring exchange interaction (which may correspond to a hard core version of the boson model with a similar ring exchange considered in Ref. [6]) did not find this novel phase, but found that new emerging ground state is a striped bond-plaquette ordered state at intermediate values of the ratio between the four-spin ring exchange and the nearest-neighbor Heisenberg exchange couplings [7].

Independent of these developments, there have been great interest in finding novel broken symmetry phases in correlated electron systems. Notable examples are the proposals of various time-reversal symmetry broken phases for the explanation of the pseudogap phase of underdoped cuprates. [8,9,10] One of these examples involve short-ranged (fluctuating) [9] or long-ranged [8] orbital antiferromagnetic order; the long-range ordered state is often called the staggered flux phase [11] or the d-density wave state [8]. This is a metallic state and characterized by alternating circulating currents in plaquettes of the square lattice while the charge density is uniform. Whether the short-range or the long-range ordered orbital antiferromagnetism is responsible for the pseudogap in cuprates has been a subject of recent debates [12,13]. Mean field theory studies of some microscopic models have shown that the orbital antiferromagnetic state appears in some part of the phase diagram [11,14]. Some ladder models also seem to allow the orbital antiferromagnetic phase [15].

Ubiquitous presence of ring exchange interactions in strongly correlated systems leads to the question of the stability of the orbital antiferromagnetic state in the presence of ring exchange processes. This is a particularly interesting question given that the large  $U$  limit of the Hubbard model possesses the ring exchange term [1]. Previous neutron scattering experiments on an undoped cuprate  $\text{La}_{2-x}\text{Sr}_x\text{CuO}_4$  suggests that the presence of ring exchange is necessary to explain the spin wave spectra [16], while the effect of ring exchange interaction may become weaker at finite concentration of mobile holes. In this paper, we investigate the effect of ring exchange process in a two-dimensional correlated electron system. In particular we would like to understand the effect of ring exchange process on the orbital antiferromagnetic state. A good starting point would be the large  $N$  limit of the  $SU(N)$  generalization of

the  $t$ - $J$  model where the orbital antiferromagnetic state is already present as a possible ground state. The ground states discovered in the large  $N$  limit may be better understood as possible ‘disordered’ states of the zero temperature magnetically ordered phases in the physical limit  $N = 2$  (such as spin antiferromagnetism), as some parameter at  $T = 0$  changes or temperature is raised. The stability of different phases in the large  $N$  limit will be reflected in those situations as well.

In this paper, we study the effect of the four-particle ring exchange interaction in the  $SU(N)$  generalization of the  $t$ - $J$ - $K$  model in the large  $N$  limit. Here  $K$  represents the strength of the four-particle ring exchange. The phase diagrams in the large  $N$  mean field theory are obtained at the half-filling and at finite hole concentration for varying strength of  $K$  and the Heisenberg exchange coupling  $J$ . We found that the ring exchange interaction in general suppresses the homogeneous orbital antiferromagnetic state and favors bond-centered dimerized phases with broken translational symmetry and/or the inhomogeneous orbital antiferromagnetic state [17] depending on the value of  $K$ .

The rest of the paper is organized as follows. In section II, the  $SU(N)$  generalization of the  $t$ - $J$ - $K$  model and the corresponding large  $N$  mean field theory are discussed. The phase diagrams for various values of  $J$  and  $K$  at the half-filling and finite hole concentration are constructed in section III. Summary of the results, discussions on possible relations to other models with ring exchange, and conclusion can be found in section IV.

## II. THE MODEL

We consider the  $t$ - $J$  model with four-particle exchange couplings on an anisotropic triangular lattice with nearest-neighbor and next-nearest-neighbor interactions:

$$\begin{aligned}
H = & -t_1 \sum_{\langle ij \rangle} c_i^\dagger c_{j\alpha} - t_2 \sum_{\langle\langle jl \rangle\rangle} c_j^\dagger c_{l\alpha} - t_3 \sum_{\langle\langle ik \rangle\rangle} c_i^\dagger c_{k\alpha} \\
& + J_1 \sum_{\langle ij \rangle} (\vec{S}_i \cdot \vec{S}_j - \frac{1}{4} n_i n_j) + J_2 \sum_{\langle\langle jl \rangle\rangle} (\vec{S}_j \cdot \vec{S}_l - \frac{1}{4} n_j n_l) + J_3 \sum_{\langle\langle ik \rangle\rangle} (\vec{S}_i \cdot \vec{S}_k - \frac{1}{4} n_i n_k) \\
& + \sum_{\langle ijkl \rangle} [K(\vec{S}_i \cdot \vec{S}_j)(\vec{S}_k \cdot \vec{S}_l) + (\vec{S}_i \cdot \vec{S}_l)(\vec{S}_j \cdot \vec{S}_k) - \lambda(\vec{S}_i \cdot \vec{S}_k)(\vec{S}_j \cdot \vec{S}_l)],
\end{aligned} \tag{1}$$

where  $c_{i\alpha}$  is the electron destruction operator of spin  $\alpha = \uparrow, \downarrow$  on site  $\mathbf{i}$ ,  $\vec{S}_i = \frac{1}{2} c_i^\dagger \vec{\sigma} c_i$  is the electron spin operator, and  $n_i = c_i^\dagger c_i$  (sum over repeated indices are assumed throughout this paper) is the electron number operator. Here  $J_1$  and  $t_1$  are the nearest-neighbor Heisenberg exchange coupling and hopping parameter while  $J_2, J_3$  and  $t_2, t_3$  are the next-nearest-neighbor Heisenberg exchange coupling and hopping parameters respectively as shown in Fig.1.  $K$  and  $\lambda$  are the strength of the four-particle exchange couplings, and the sum in the four-particle exchange is over all non-overlapping plaquettes labelled clockwise by the sites  $\mathbf{i}, \mathbf{j}, \mathbf{k}$  and  $\mathbf{l}$  (see Fig.1). Note that at  $\lambda = K$ , the four-particle exchange terms correspond to the conventional ring exchange process [3]. To get further insight, we consider more general four-particle exchange interactions by treating  $\lambda$  as an independent free parameter [18]. By doing so, we may at first investigate several simple limits where the model is easier to solve and the results in these limits can provide us useful guidance in studying the effect of various four-particle exchange couplings (including the ring exchange) on the orbital antiferromagnetic state. Then we will come back later to the case of more interesting and physical ring exchange coupling.

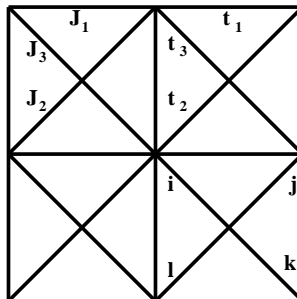


FIG. 1. Anisotropic triangular lattice with three types of the bonds.

To make a progress, we apply a large- $N$  approach by generalizing the spin symmetry from  $SU(2)$  to  $SU(N)$  [11,19].  $N = 2$  corresponds to the physical  $SU(2)$  spin-1/2 system. The large- $N$  approach has been applied to various strongly correlated systems [11,19,20]. One advantage of this approach is that the mean field solutions become exact in the limit of  $N \rightarrow \infty$  and thus it is possible to systematically calculate corrections in powers of  $1/N$ .

Let us briefly describe the  $SU(N)$  generalization of the Hamiltonian in Eq.1. In the  $SU(2)$  case, we can express the Hamiltonian in terms of fermionic operators by use of the following identity [11]:

$$\vec{S}_i \cdot \vec{S}_j = -\frac{1}{2}(c_i^\dagger c_{j\alpha})(c_j^\dagger c_{i\beta}) + \frac{1}{2}n_i - \frac{1}{4}n_i n_j, \quad (2)$$

The  $SU(N)$  generalization of the  $SU(2)$  Hamiltonian is obtained by simply letting the spin index  $\alpha$  run from 1 to  $N$ . We apply the slave-boson method to impose the constraint in the Hilbert space. In the slave-boson representation, the spins are represented by fermions  $f_\alpha$ ,  $\alpha = 1 \cdots N$  which transform under the fundamental representation of  $SU(N)$ ; the holes are represented by spinless bosons  $b_i$  where  $c_{i\alpha} = f_{i\alpha} b_i^\dagger$ . The local constraint is given by [21]:

$$f_i^\dagger f_{i\alpha} + b_i^\dagger b_i = \frac{N}{2}. \quad (3)$$

In the  $N \rightarrow \infty$  limit and at zero temperature, the average hole concentration  $\delta$  can be obtained from [21]

$$\frac{1}{N_s} \sum_i < f_i^\dagger f_{i\alpha} > = \frac{N}{2}(1 - \delta), \quad (4)$$

where  $N_s$  is the total number of sites in the system. In this paper, we only consider the case with uniform charge distribution which excludes the possibility of site-centered charge density wave or stripe state that was found in some related models [21]. Investigation of the possibility of charge stripe phases is an interesting and yet a separate topic which is beyond the scope of this paper. Based on this assumption, the hole concentration is given by  $\delta$ , and the electron density operator  $n_{i\alpha}$  is a constant  $c$  number,  $n_i = \frac{N}{2}(1 - \delta)$ . Note that there is exactly one electron per site in the limit of the physical  $SU(2)$  spin-1/2 case at the half-filling.

The  $SU(N)$  generalization of the Hamiltonian in Eq.1 is therefore given by:

$$\begin{aligned} H_{SU(N)} = & -t_1 \delta \sum_{\langle ij \rangle} f_i^\dagger f_{j\alpha} - t_2 \delta \sum_{\langle\langle jl \rangle\rangle} f_j^\dagger f_{l\alpha} - t_3 \delta \sum_{\langle\langle ik \rangle\rangle} f_i^\dagger f_{k\alpha} \\ & - \frac{J_1^e}{N} \sum_{\langle ij \rangle} |f_i^\dagger f_{j\alpha}|^2 - \frac{J_2^e}{N} \sum_{\langle\langle jl \rangle\rangle} |f_j^\dagger f_{l\alpha}|^2 - \frac{J_3^e}{N} \sum_{\langle\langle ik \rangle\rangle} |f_i^\dagger f_{k\alpha}|^2 \\ & + \sum_{\langle ijkl \rangle} \left[ \frac{2K}{N^3} (|f_i^\dagger f_{j\alpha}|^2 |f_k^\dagger f_{l\beta}|^2 + |f_i^\dagger f_{l\alpha}|^2 |f_j^\dagger f_{k\beta}|^2) - \frac{\lambda}{N^3} |f_i^\dagger f_{k\alpha}|^2 |f_j^\dagger f_{l\beta}|^2 \right], \end{aligned} \quad (5)$$

where the Heisenberg exchange couplings  $J_{ij}$  have been renormalized by the ring exchange interactions leading to the effective couplings:  $J_1^e = J_1(1 - \frac{K}{2J_1}(1 - \delta)^2)$ ,  $J_2^e = J_2(1 + \frac{\lambda}{4J_2}(1 - \delta)^2)$ , and  $J_3^e = J_3(1 + \frac{\lambda}{4J_3}(1 - \delta)^2)$ . Note that we rescale both  $J_{ij}$  and  $K$  by a factor of  $\frac{2}{N}$  so that the Hamiltonian is of the order  $N$ . [11]. Also, we have dropped the constant terms involving  $n_i$  and  $n_i n_j$  in the Hamiltonian.

The above Hamiltonian contains eight- and four-fermion interactions. We may decouple these interactions into quadratic interactions by applying the Hubbard-Stratonovich transformations. We then perform the functional integration over the Hubbard-Stratonovich fields in a saddle-point approximation [11]. The key point in the large- $N$  approach is that the saddle-point solution becomes exact in the  $N \rightarrow \infty$  limit. The factorization of the spin-spin interactions can be done in two stages [11]. We first break up the eight-fermion terms by introducing real Hubbard-Stratonovich fields  $\Phi_{ij}$ :

$$\begin{aligned} \frac{2K}{N^3} |f_i^\dagger f_{j\alpha}|^2 |f_k^\dagger f_{l\beta}|^2 & \rightarrow N \left[ -\frac{1}{2K} \Phi_{ij} \Phi_{kl} - \frac{\Phi_{ij}}{N^2} |f_k^\dagger f_{l\beta}|^2 - \frac{\Phi_{kl}}{N^2} |f_i^\dagger f_{j\alpha}|^2 \right] \\ \frac{-2\lambda}{N^3} |f_i^\dagger f_{k\alpha}|^2 |f_j^\dagger f_{l\beta}|^2 & \rightarrow N \left[ \frac{1}{2\lambda} \Phi_{ik} \Phi_{jl} - \frac{\Phi_{ik}}{N^2} |f_j^\dagger f_{l\beta}|^2 - \frac{\Phi_{jl}}{N^2} |f_i^\dagger f_{k\alpha}|^2 \right] \end{aligned} \quad (6)$$

At the saddle-point  $\Phi_{ij}$  fields take the following values:

$$\begin{aligned} \Phi_{ij} &= -\frac{2K}{N^2} < |f_i^\dagger f_{j\alpha}|^2 > \\ \Phi_{ik} &= \frac{2\lambda}{N^2} < |f_i^\dagger f_{k\alpha}|^2 >, \end{aligned} \quad (7)$$

where  $\Phi_{\mathbf{ij}}$  and  $\Phi_{\mathbf{ik}}$  represent the fields along the nearest-neighbor and next-nearest-neighbor sites respectively.

After the first Hubbard-Stratonovich transformation, the Hamiltonian now still contains four-fermion interactions. We can decouple these terms by introducing the complex Hubbard-Stratonovich fields  $\chi_{\mathbf{ij}}$ :

$$\begin{aligned} -J_1^e(1 + \frac{2\Phi_{\mathbf{kl}}}{J_1^e})|f_i^{\dagger\alpha} f_{j\alpha}|^2 &\rightarrow (1 + \frac{2\Phi_{\mathbf{kl}}}{J_1^e})(\frac{|\chi_{\mathbf{ij}}|^2}{J_1^e} - \frac{\chi_{\mathbf{ij}}^*}{N} f_i^{\dagger\alpha} f_{j\alpha} + H.c.), \\ -J_2^e(1 + \frac{\Phi_{\mathbf{ik}}}{J_2^e})|f_j^{\dagger\alpha} f_{l\alpha}|^2 &\rightarrow (1 + \frac{\Phi_{\mathbf{ik}}}{J_2^e})(\frac{|\chi_{\mathbf{jl}}|^2}{J_2^e} - \frac{\chi_{\mathbf{jl}}^*}{N} f_j^{\dagger\alpha} f_{l\alpha} + H.c.), \\ -J_3^e(1 + \frac{\Phi_{\mathbf{jl}}}{J_3^e})|f_i^{\dagger\alpha} f_{k\alpha}|^2 &\rightarrow (1 + \frac{\Phi_{\mathbf{jl}}}{J_3^e})(\frac{|\chi_{\mathbf{ik}}|^2}{J_3^e} - \frac{\chi_{\mathbf{ik}}^*}{N} f_i^{\dagger\alpha} f_{k\alpha} + H.c.). \end{aligned} \quad (8)$$

where  $\chi_{\mathbf{ij}}$  fields have the following saddle-point values [11]:

$$\chi_{\mathbf{ij}} = \frac{J_{\mathbf{ij}}^e}{N} \langle f_i^{\dagger\alpha} f_{j\alpha} \rangle. \quad (9)$$

After two Hubbard-Stratonovich transformations, the Hamiltonian is now quadratic in fermion operators. Note that at the saddle-point  $\Phi_{\mathbf{ij}}$  and  $\chi_{\mathbf{ij}}$  fields have the following relations:

$$\begin{aligned} \Phi_{\mathbf{ij}} &= -\frac{2K}{(J_{\mathbf{ij}}^e)^2} |\chi_{\mathbf{ij}}|^2 \\ \Phi_{\mathbf{ik}} &= \frac{2\lambda}{(J_{\mathbf{ik}}^e)^2} |\chi_{\mathbf{ik}}|^2, \end{aligned} \quad (10)$$

where  $\mathbf{ij}$  and  $\mathbf{ik}$  again are the nearest-neighbor and next-nearest-neighbor sites respectively. Therefore, we can express the mean-field Hamiltonian purely in terms of  $\chi$ -fields. After integrating out the fermions, the resulting free energy is given by [11]:

$$\begin{aligned} \frac{E_{MF}}{N} &= \sum_{\langle \mathbf{ijkl} \rangle} [-\frac{6K}{(J_1^e)^4} (|\chi_{\mathbf{ij}}|^2 |\chi_{\mathbf{kl}}|^2 + |\chi_{\mathbf{il}}|^2 |\chi_{\mathbf{jk}}|^2) + \frac{6K}{(J_2^e)^2 (J_3^e)^2} |\chi_{\mathbf{ik}}|^2 |\chi_{\mathbf{jl}}|^2] \\ &+ \sum_{\langle \mathbf{ij} \rangle} \frac{|\chi_{\mathbf{ij}}|^2}{J_1^e} + \sum_{\langle \langle \mathbf{jl} \rangle \rangle} \frac{|\chi_{\mathbf{jl}}|^2}{J_2^e} + \sum_{\langle \langle \mathbf{ik} \rangle \rangle} \frac{|\chi_{\mathbf{ik}}|^2}{J_3^e} \\ &- \frac{1}{\beta} \sum_{\mathbf{k}} \ln\{1 + e^{[-\beta(\omega_{\mathbf{k}} - \mu)]}\}, \end{aligned} \quad (11)$$

where  $\mu$  is the chemical potential which fixes the number of the fermions,  $\beta = \frac{1}{k_B T}$  is the inverse of the temperature,  $\omega_{\mathbf{k}}$  are the eigenvalues of the following Hamiltonian  $H_1$ :

$$\begin{aligned} \frac{H_1}{N} &= -t_1 \delta \sum_{\langle \mathbf{ij} \rangle} f_i^{\dagger\alpha} f_{j\alpha} - t_2 \delta \sum_{\langle \langle \mathbf{jl} \rangle \rangle} f_j^{\dagger\alpha} f_{l\alpha} - t_3 \delta \sum_{\langle \langle \mathbf{ik} \rangle \rangle} f_i^{\dagger\alpha} f_{k\alpha} \\ &+ \sum_{\langle \mathbf{ijkl} \rangle} [(1 - \frac{4K|\chi_{\mathbf{kl}}|^2}{(J_1^e)^3}) (-\frac{\chi_{\mathbf{ij}}^*}{N} f_i^{\dagger\alpha} f_{j\alpha} + H.c.) \\ &+ (1 - \frac{4K|\chi_{\mathbf{il}}|^2}{(J_1^e)^3}) (-\frac{\chi_{\mathbf{jk}}^*}{N} f_j^{\dagger\alpha} f_{k\alpha} + H.c.) \\ &+ (1 + \frac{2\lambda|\chi_{\mathbf{ik}}|^2}{J_2^e (J_3^e)^2}) (-\frac{\chi_{\mathbf{jl}}^*}{N} f_j^{\dagger\alpha} f_{l\alpha} + H.c.) \\ &+ (1 + \frac{2\lambda|\chi_{\mathbf{jl}}|^2}{J_3^e (J_2^e)^2}) (-\frac{\chi_{\mathbf{ik}}^*}{N} f_i^{\dagger\alpha} f_{k\alpha} + H.c.)]. \end{aligned} \quad (12)$$

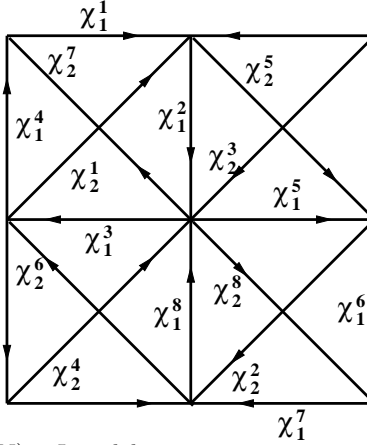


FIG. 2. The  $2 \times 2$ -site unit cell of the  $SU(N)$   $t$ - $J$  model on an anisotropic triangular lattice. Arrows indicate the orientation of the complex-valued  $\chi_{ij}$  fields.

Note that at the half-filling, the mean-field Hamiltonian is invariant under local  $U(1)$  gauge transformations as long as the  $\chi$ -fields transform as gauge fields [11]:  $\chi_{ij}(\tau) \rightarrow e^{i[\theta_i(\tau) - \theta_j(\tau)]} \chi_{ij}(\tau)$ . Away from half-filling, this local  $U(1)$  gauge symmetry is broken down to only the global  $U(1)$  gauge symmetry reflecting the conservation of total charge. The ground state of the system is found by solving the saddle-point equations,  $\frac{\partial E_{MF}}{\partial \chi_{ij}} = 0$ , for  $\chi_{ij}$ -fields. Extrema of  $E_{MF}$  are found numerically with the simplex-annealing method [22]. To make progress in solving the model, we make the assumption that spontaneous symmetry breaking, if it occurs, does not lead to a unit cell larger than 4 sites. Our choice of unit cell is shown in Fig.2. The  $2 \times 2$  unit cell requires 16 different complex-valued  $\chi$ -fields (8  $\chi_1$ -fields on the square and 8  $\chi_2$ -fields along the diagonals). We work with a lattice of  $40 \times 40$  sites and check that this is sufficiently large to accurately represent the thermodynamic limit. We check all the saddle-point solutions and make sure that the ground state is the one with the lowest free energy.

### III. ZERO TEMPERATURE PHASE DIAGRAM

Possible ground states of the system may be classified into several different phases which are characterized by the symmetry of the  $\chi_{ij}$ -fields at the saddle-point. In the half-filled ( $\delta = 0$ ) case, it is important to classify the phases in a gauge-invariant fashion because there are many gauge-equivalent saddle-points. There are two important gauge-invariant quantities [20]:

- (i) The squared amplitude  $|\chi_{ij}|^2$  which is proportional to the spin-spin correlation function  $\langle \vec{S}_i \cdot \vec{S}_j \rangle$ . Modulations in  $|\chi|$  signal the presence of a bond-centered dimerization.
- (ii) The plaquette operator  $\Pi \equiv \chi_{12}\chi_{23}\chi_{34}\chi_{41}$ , where 1, 2, 3, and 4 are sites on the corners of a unit plaquette. By identifying the phase of  $\chi$  as a spatial gauge field it is clear that the plaquette operator is gauge-invariant, and its phase measures the amount of magnetic flux penetrating the plaquette [11]. Different saddle points are therefore gauge equivalent if the plaquette operator has the same expectation value, even though the  $\chi$ -fields may be different. At half-filling the flux always equals to 0 or  $\pi \pmod{2\pi}$ , so one can always choose a gauge such that all the  $\chi$ -fields are purely real [11].

Away from the  $\delta = 0$  limit, the saddle-point solutions are further classified in terms of whether or not they break time-reversal symmetry ( $\hat{T}$ ) where the plaquette operator has a nontrivial phase other than 0 or  $\pi$ . The  $\hat{T}$ -breaking state will generate real orbital currents going through the plaquettes in an alternating fashion [11,20]. Finally, as there are eight independent parameters ( $t_1, t_2, t_3, J_1, J_2, J_3, K$ , and  $\lambda$ ) the phase diagram lives in a seven-dimensional space of their dimensionless ratios. Since we are interested in how the four-particle exchange couplings may affect the orbital antiferromagnetic state, we reduce the parameter space to a more manageable two-dimensional section by fixing the ratios of  $J_1^e/J_2^e$ ,  $J_1^e/J_3^e$ ,  $t_1/t_2$ ,  $t_1/t_3$ , and  $K/\lambda$  such that the orbital antiferromagnetic state appears as one of the ground states of the system. Then by varying  $J_1^e/t_1$  (or  $J_2^e/t_2$ ) and  $K/J_1^e$  (or  $\lambda/J_2^e$ ) we explore the phase diagram in a two-dimensional space. We summarize the phases which appear in the phase diagram in the following subsections.

### A. Half-filling ( $\delta = 0$ )

We find that in this limit the ground states are always dimerized in one way or another with spatial modulations in spin-spin correlations. Although the staggered flux phase (that becomes the orbital antiferromagnetic state at non-zero hole concentration) is a saddle-point solution, its free energy is always higher than the dimerized ground states. To see this more clearly, we plot the free energy as a function of the four-particle exchange parameter  $K$  in the square lattice limit ( $J_2^e = J_3^e = 0$ ) with  $\lambda = 0$  (see Fig.6). We compare the free energies of the saddle-point solutions which are competing with each other to be the true ground state. In this limit, we find the following competing phases:

#### Dimer phase

This is a fully dimerized phase which exhibits spin-Peierls order:  $|\chi_1^1| = |\chi_1^5| \neq 0$ , and all other  $\chi$ -fields are zero; See Fig.3 for a sketch [20]. It breaks the translational symmetry and have spatial modulations in spin-spin correlations. In fact, the system breaks up into decoupled dimerized spin chains. It is an insulating phase as there is a large gap in the energy spectrum at the Fermi energy.

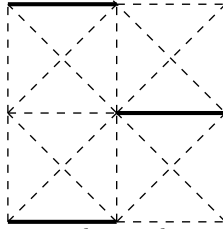


FIG. 3. The dimer phase with decoupled dimerized spin chains. Dark solid links indicate nonzero spin-spin correlations and dash links have zero spin-spin correlations.

#### Box phase

This insulating phase breaks the translational symmetry and consists of isolated plaquettes with enhanced spin-spin correlations [20,23,24]. The  $\chi_1$ -fields are either 0 or complex with  $|\chi_1^1| = |\chi_1^2| = |\chi_1^3| = |\chi_1^4| \neq 0$ , and  $|\chi_1^5| = |\chi_1^6| = |\chi_1^7| = |\chi_1^8| = 0$ . All  $\chi_2$  fields are zero. See Fig.4 for a sketch. This phase is similar to the fully dimerized phase as the magnitudes of the  $\chi_1$ -fields modulate on the lattice. The box phase does not break the time-reversal symmetry as the phase of the plaquette product  $\chi_1^1\chi_1^2\chi_1^3\chi_1^4$  is either 0 or  $\pi$ . There are no real orbital currents circulating since we can always choose a gauge to make  $\chi$ -fields real.

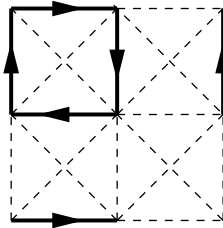


FIG. 4. Box phase with 0 or  $\pi$  flux around the plaquette. Dark solid links indicate nonzero spin-spin correlations and dash links have zero spin-spin correlations. The arrows indicate the complex-valued  $\chi$ -fields.

#### Staggered Flux Phase

All  $\chi_1$ -fields are equal, with an imaginary component in general, and all  $\chi_2$ -fields along the diagonals are zero; see Fig.5 for a sketch. Like the box phase, the staggered flux phase at the half-filling does not break  $\hat{T}$ -symmetry as the phase of the plaquette operator is either 0 or  $\pi$ . We can always make a gauge transformation such that all  $\chi_1$ -fields are real. There are therefore no real orbital currents circulating around the plaquettes. This phase is semi-metallic as the density of states is small, and in fact vanishes linearly at the Fermi energy. The gauge fluctuations at sufficiently small- $N$  are expected to drive the staggered flux phase into a Néel-ordered state [25].

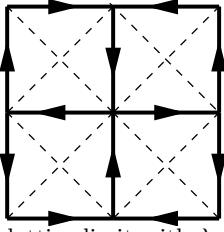


FIG. 5. Staggered flux phase in the square lattice limit with  $\lambda = 0$ . The dark links on the square indicate strong spin-spin correlations and the dash links along the diagonals have zero spin-spin correlation. The arrows indicate the orientation of the complex-valued  $\chi$ -fields. At half-filling, there is no real circulating orbital currents since the flux around the plaquette is either 0 or  $\pi$ . Away from half-filling, however, the flux around the plaquette is neither 0 nor  $\pi$ . There are therefore real orbital currents in this case circulating in an antiferromagnetic fashion as indicated by the arrows; thus it is an orbital antiferromagnet.

We plot the free energy as a function of  $K/J_1^e$  as shown in Fig.6. We can see that the box and the dimer phases are the ground states for  $K < 0$  and  $K > 0$  respectively. The staggered flux phase is not the ground state in both cases. We have also checked the free energy as a function of  $\lambda/J_2^e$  in the other extreme limit where  $J_1^e = 0$  and  $K = 0$  (two inter-penetrating square lattice limit). We also find that the staggered flux phase is not the ground state for both  $\lambda > 0$  and  $\lambda < 0$ .

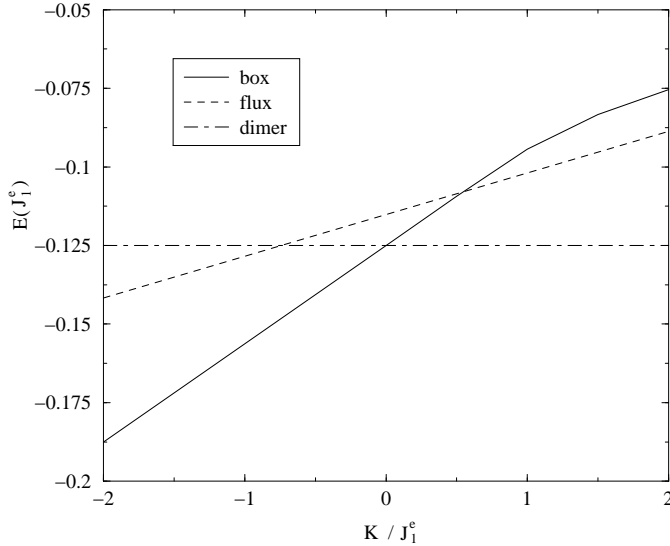


FIG. 6. Free energy of the half-filled  $t-J$  model on the square lattice as a function of  $K/J_1^e$  for three competing saddle-point solutions. Note that the dimer and box phase are degenerate ground states at  $K = 0$ .

From our results at the half-filling, it is clear that the four-particle exchange actually favors the dimerized phases over the staggered flux phase. The dimerized state which breaks translational symmetry is in fact a bond-centered charge density wave state [11]. Recent Monte Carlo study of the quantum XY model with ring exchange indicates plaquette (stripe) order which is also a bond-centered charge density wave state as the ring exchange coupling exceeds the critical value [7]. In fact, the box phase in our model in the square lattice limit with  $K < 0$  looks very similar to the plaquette phase in the quantum XY model mentioned above. Although there are differences between the XY model and our  $t-J$  model, these two models share the same structure of the spin-spin interactions and have similar ground states. Note that the four-particle exchange and the ring exchange couplings share the similar form of spin-spin interactions. We therefore expect that even though the staggered flux phase is not a ground state in our model at half-filling, our result at half-filling can still give us an important clue about the effects of the ring exchange couplings on the system at finite doping where the staggered flux phase does appear to be a ground state. Now we proceed to solve our model at finite doping.

## B. Nonzero doping ( $\delta = 0.05$ )

Unlike the half-filled case where the staggered flux phase is never a ground state, at nonzero doping the hopping terms are expected to stabilize the staggered flux phase [11]. We find the staggered flux phase is indeed the ground state of our system over a range of  $J_1^e/t_1$  ratio. From our results at the half-filling, however, we know that the four-particle exchange favors dimerization over the staggered flux phase. We find it is also the case at finite doping. There is therefore the competition between the hopping terms and the four-particle exchange couplings which results in an interesting phase diagram.

Again, we first work on the phase diagrams of two simple limits where the staggered flux phase appears as a stable ground state. We then move on to the more interesting ring exchange limit where all the couplings are nonzero. Here, we fix the doping concentration  $\delta$  to be 0.05.

### 1. Square lattice limit with $\delta = 0.05$

As shown in Fig.10, we find the following phases in our phase diagram:

#### Dimer phase

This dimer phase breaks translational symmetry and it exists at large  $J_1^e/t_1$  and positive  $K/J_1^e$  ratio. This phase is a partially dimerized phase as  $|\chi_1^1| = |\chi_1^5| > |\chi_1^2| = |\chi_1^6| > |\chi_1^3| = |\chi_1^7| > |\chi_1^4| = |\chi_1^8|$ . All  $\chi_2$ -fields are zero. See Fig.7 for a sketch.

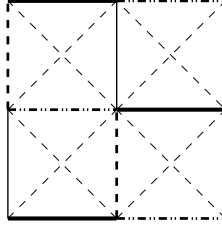


FIG. 7. The one-dimensional partially dimerized phase at  $\delta = 0.05$ . Dark solid links indicate strong spin-spin correlations, light solid and dark dash links indicate weak spin-spin correlations. The  $\chi_2$ -fields on the diagonals are zero.

#### Box phase

This box phase next to the dimer phase also breaks the translational symmetry and exists at large  $J_1^e/t_1$  ratio and at negative or small positive  $K/J_1^e$  ratio. This phase is very similar to the box phase at half-filling except now it is partially dimerized. All  $\chi_1$ -fields are complex and  $|\chi_1^1| = |\chi_1^2| = |\chi_1^3| = |\chi_1^4| > |\chi_1^5| = |\chi_1^6| = |\chi_1^7| = |\chi_1^8|$ . The imaginary parts of  $\chi_1$ -fields have the similar relation:  $Im(\chi_1^1) = Im(\chi_1^2) = Im(\chi_1^3) = Im(\chi_1^4) > Im(\chi_1^5) = Im(\chi_1^6) = Im(\chi_1^7) = Im(\chi_1^8)$ . All  $\chi_2$ -fields along the diagonals are zero. This box phase at finite doping breaks the time-reversal symmetry as the phase of the plaquette product is neither 0 nor  $\pi$  in general. There are *real* orbital currents circulating around the plaquette. This corresponds to an inhomogeneous orbital antiferromagnetic state. See Fig.8 for a sketch.

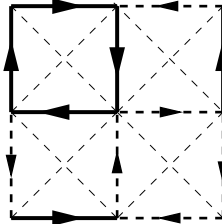


FIG. 8. Box phase on the square lattice at  $\delta = 0.05$ . The flux around the plaquette is neither 0 nor  $\pi$ . Dark solid links indicate larger magnitudes of the  $\chi_1$ -fields or stronger spin-spin correlations and dark dash links indicate smaller magnitudes of the  $\chi_1$ -fields or weaker spin-spin correlations. The arrows indicate the complex-valued  $\chi_1$ -fields and also the directions of the orbital currents. The  $\chi_2$ -fields along the diagonals are zero. We have checked that the orbital currents are conserved at each site.

#### Staggered flux phase (Homogeneous orbital antiferromagnetic state)

This phase exists at intermediate range of  $J_1^e/t_1$  ratio. It is very similar to the staggered flux phase at half-filling except that now it breaks  $\hat{T}$ -symmetry as the phase of the plaquette operator is neither 0 nor  $\pi$ ; see Fig.5 for a sketch.



There are therefore real orbital currents circulating around the plaquette. Note that unlike the box phase, the  $\chi$ -fields in the staggered flux phase have the same magnitude.

### Uniform phase

This phase exists at small  $J_1^e/t_1$  ratio where all  $\chi_1$ -fields become negative real numbers and  $\chi_1^1 = \chi_1^2 = \dots = \chi_1^8$ , and all  $\chi_2$ -fields are zero. See Fig.9 for a sketch. This phase preserves  $\hat{T}$ -symmetry and since all  $\chi$ -fields are real, they simply renormalize the hopping parameter  $t_1$ . The uniform phase is therefore a metallic Fermi liquid. Spin-spin correlations in the uniform phase decay with an inverse power law of the separation [20].

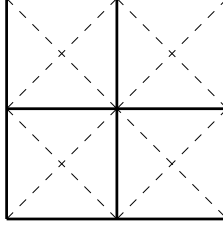


FIG. 9. Uniform phase in the square lattice limit. This phase does not have broken symmetries and it is a Fermi liquid.

As shown in Fig.10, the general features of the phase diagram suggest that the region of the staggered flux phase (homogeneous orbital antiferromagnetic state) becomes narrower and that of the dimerized phase and/or the box phase (inhomogeneous orbital antiferromagnetic state) becomes wider as we increase both the positive and negative  $K/J_1^e$  ratios. This is consistent with what we find at the half-filled case where the four-particle exchange couplings enhance dimerization and suppress the staggered flux phase. Also, for a fixed  $J_1^e/t_1$  ratio, the ground state may change from the box phase to the staggered flux phase and finally to the dimer phase as the ratio of  $K/J_1^e$  is changed from negative to positive values.

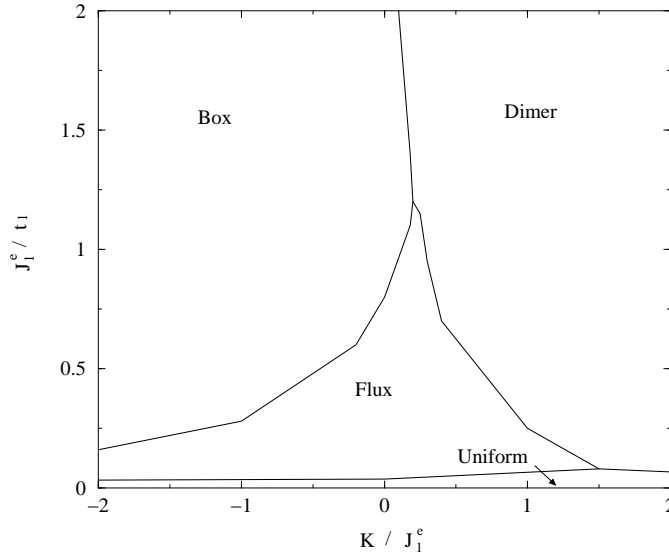


FIG. 10. Zero temperature phase diagram of the  $SU(N)$   $t$ - $J$  model in the square lattice limit as a function of  $J_1^e/t_1$  and  $K/J_1^e$ .

## 2. Two inter-penetrating square lattice limit with $\delta = 0.05$

In this limit, the ground state phases are classified as follows:

### 1D dimer phase

This phase is a ‘one-dimensional’ partially dimerized phase which breaks up the system into nearly decoupled dimerized spin chains along one of the two diagonal directions:  $|\chi_2^1| > |\chi_2^3| > |\chi_2^4| = |\chi_2^7| = |\chi_2^8| > |\chi_2^2| = |\chi_2^5| = |\chi_2^6|$  (see Fig.11). This phase is the ground state for  $\lambda < 0$ . Note that at half-filling, this phase is completely dimerized:  $|\chi_2^1| = |\chi_2^3| \neq 0$ , and all other  $\chi$ -fields are zero.

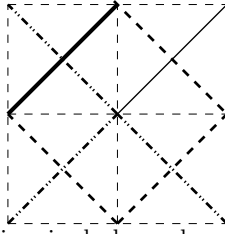


FIG. 11. The ‘one-dimensional’ partially dimerized phase along the diagonals. Solid links indicate strong spin-spin correlations and dark dash links indicate weak spin-spin correlations. The  $\chi_1$ -fields on the square are zero.

### 2D dimer phase

This phase is a ‘two-dimensional’ partially dimerized phase which breaks up the system into nearly decoupled dimerized spin chains along both of the diagonal directions:  $|\chi_2^1| > |\chi_2^7| > |\chi_2^3| = |\chi_2^4| = |\chi_2^8| > |\chi_2^2| = |\chi_2^5| = |\chi_2^6|$  (see Fig.12). This phase is the ground state for  $\lambda > 0$ . Note that at half-filling, this phase is completely dimerized:  $|\chi_2^1| = |\chi_2^7| \neq 0$ , and all other  $\chi$ -fields are zero.

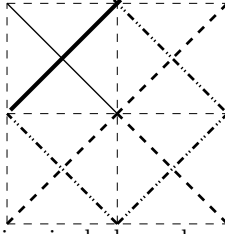


FIG. 12. The ‘two-dimensional’ partially dimerized phase along the diagonals. Solid links indicate strong spin-spin correlations and dark dash links have weak spin-spin correlations. The  $\chi_1$ -fields on the square are zero.

### Staggered flux phase (Homogeneous orbital antiferromagnetic phase)

The staggered flux phase exists at intermediate values of  $J_2^e/t_2$ . All  $\chi_2$ -fields are equal, with an imaginary component in general, and all  $\chi_1$ -fields on the square are zero (see Fig.13). This phase is very similar to the staggered flux phase on the square lattice except that now the flux goes through the plaquettes of two square lattices (rotated by  $45^\circ$ ) inter-penetrating to each other. Like staggered flux phase on the square lattice at nonzero doping, this phase also breaks  $\hat{T}$ -symmetry and there are real orbital currents running through the two inter-penetrating plaquettes as the phase of the plaquette operator is neither 0 nor  $\pi$ .

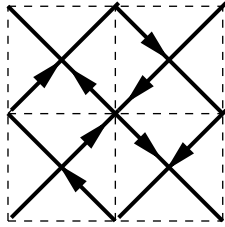


FIG. 13. Staggered flux phase in the two inter-penetrating square lattice limit. The dark links along the diagonals indicate strong spin-spin correlations and the dash links on the square have zero spin-spin correlation. The arrows indicate the orientation of the complex-valued  $\chi$ -fields. The lattice can be also viewed in this limit as if there are two inter-penetrating square lattices rotated by  $45^\circ$ . At half-filling, there is no real circulating orbital currents since the flux around the plaquette of these rotated square lattices is either 0 or  $\pi$ . Away from half-filling, however, the flux is neither 0 nor  $\pi$ . Therefore, there are real orbital currents circulating in an antiferromagnetic fashion as indicated by the arrows.

### Uniform phase

This is the ground state at small  $J_2^e/t_2$  ratio. This metallic phase is similar to the uniform phase in the square lattice limit except that now  $\chi_2^1 = \dots = \chi_2^8 \neq 0$  and all  $\chi_1$ -fields are zero (see Fig.14).

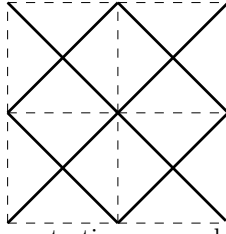


FIG. 14. Uniform phase in the two inter-penetrating square lattice limit at  $\delta = 0.05$ . This phase does not have broken symmetries and it is a Fermi liquid.

We again plot the phase diagram as a function of  $J_2^e/t_2$  and  $\lambda/J_2^e$  as shown in Fig.15. The phase diagram suggests that the region of the staggered flux phase becomes narrower and that of the dimerized phases becomes wider as both the positive and negative  $\lambda/J_2^e$  ratios are increased. We reach the same conclusion as in the square lattice limit; the four-particle exchange couplings enhance dimerization and suppress the staggered flux phase (homogeneous orbital antiferromagnetic state). Also, for a fixed  $J_1^e/t_1$  ratio, there are quantum phase transitions between the 1D dimer phase and the staggered flux phase as well as between staggered flux phase and the 2D dimer phase as the ratio of  $\lambda/J_2^e$  is varied.

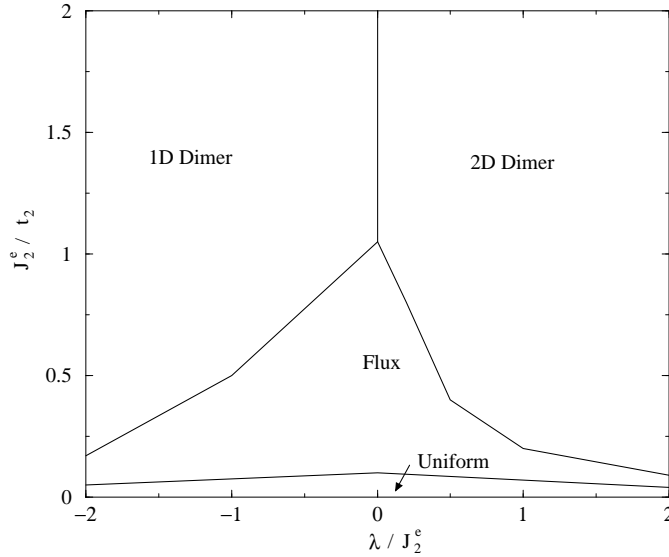


FIG. 15. Zero temperature phase diagram of the  $SU(N)$   $t$ - $J$  model in the limit of  $J_1^e = t_1 = K = 0$ , and  $J_2^e = J_3^e$ ,  $t_2 = t_3$ . The doping concentration  $\delta = 0.05$ .

In addition to the above two extreme limits, we also look at the more interesting ring exchange limit where  $K = \lambda$  and all  $J_{ij}$  and  $t_{ij}$  are nonzero. We explore a wide range of the parameter space and find that the staggered flux phase only exists in the region close to the above two extreme limits. It is expected because the staggered flux phase is suppressed by geometrical frustration effect in other regions of the phase diagram [20]. We therefore restrict our attention to the parameter space close to these two limits where the staggered flux phase exists as a stable ground state.

The phase diagrams of the system close to the square lattice limit and to the limit of two inter-penetrating square lattice are shown in Fig.16 and Fig.17 respectively. They are very similar to the phase diagrams in their corresponding extreme limits except for the shifting of the phase boundaries. It is clear from our phase diagrams that the ring exchange coupling suppresses the homogeneous orbital antiferromagnetic state and favors the dimerized and/or inhomogeneous orbital antiferromagnetic state (box phase).

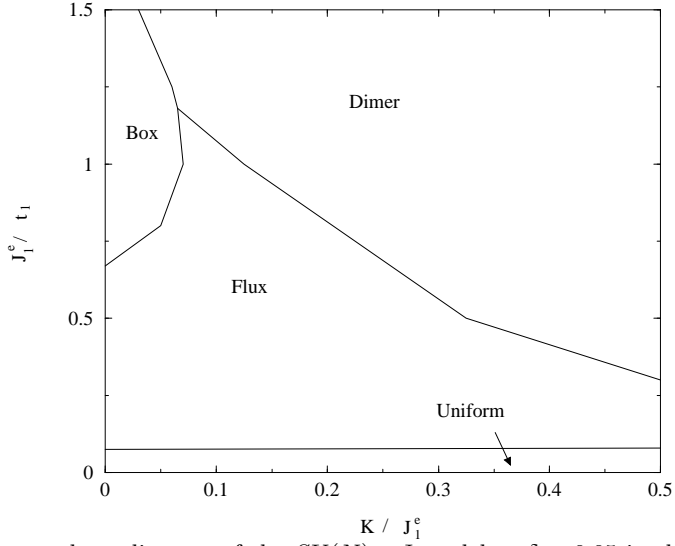


FIG. 16. Zero temperature phase diagram of the  $SU(N)$   $t$ - $J$  model at  $\delta = 0.05$  in the ring exchange ( $K = \lambda$ ) limit. Here,  $J_2^e/J_1^e = J_3^e/J_1^e = 0.5$  and  $t_2/t_1 = t_3/t_1 = 0.1$ . All the phases here are very similar to the corresponding phases in the square lattice limit except that now the  $\chi_2$ -fields along the diagonals take small nonzero real values due to frustration.

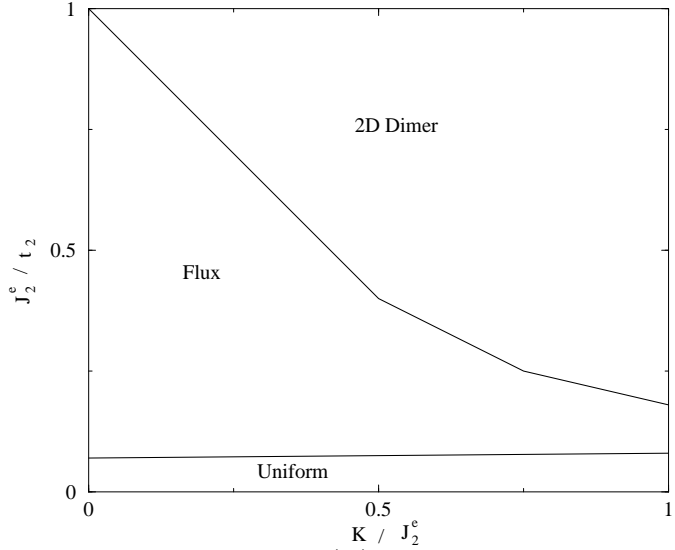


FIG. 17. Zero temperature phase diagram of the  $SU(N)$   $t$ - $J$  model at  $\delta = 0.05$  in the ring exchange ( $K = \lambda$ ) limit. Here,  $J_1^e/J_2^e = J_1^e/J_3^e = 0.25$  and  $t_1/t_2 = t_1/t_3 = 0.5$ . All the phases here are very similar to the corresponding phases in the limit of two inter-penetrating square lattice except that now the  $\chi_1$ -fields on the square take small nonzero real values due to the nonzero couplings on the square links.

#### IV. CONCLUSION

In this paper, we studied the  $t$ - $J$  model with four-particle exchange couplings given by Eq.1 on an anisotropic triangular lattice as shown in Fig.1. Even though the usual ring exchange limit corresponds to  $K = \lambda$  in Eq.1, we consider a more general model with  $K \neq \lambda$  in order to get further insights. The large- $N$  mean field theory via the  $SU(N)$  generalization of the model is used to construct various phase diagrams. The mean field ground states in the  $N \rightarrow \infty$  limit can be classified using the link variables  $\chi_{ij}$  given by Eq.9. The relevant link variables are shown in Fig.2.

We are mostly interested in the effect of the four-particle exchange couplings on the orbital antiferromagnetic state (staggered flux phase) that exists in some parts of the large parameter space of the model. It is found that it is useful to first consider two extreme limits; the square lattice limit (all the parameters describing the processes between the

next-nearest-neighbor sites are zero) and the limit of inter-penetrating square lattice (all the parameters describing the processes between the nearest-neighbor sites are zero). This is mainly because, even in the ring exchange limit  $K = \lambda$ , the staggered flux phase exists as a stable ground states near these two limits; some small nonzero next-nearest-neighbor (nearest-neighbor) hopping and Heisenberg exchange couplings about the square lattice limit (the inter-penetrating square lattice limit). We studied these two extreme cases as well as the conventional ring exchange limit at half-filling and a finite hole concentration.

Our results can be summarized as follows. In the half-filled case ( $\delta = 0$ ), Fig.6 shows the comparison of saddle-point energies of various phases in the square lattice limit. In this case, the staggered flux phase is never a ground state and either the fully dimerized phase or the box phase is the ground state. One can see from Fig.6 that the difference between the saddle-point energies of the staggered flux phase and the ground state (dimerized/box phase) becomes larger for large  $|K|$  and/or  $|\lambda|$ . At a finite hole concentration ( $\delta = 0.05$ ), the phase diagrams in the square lattice and the inter-penetrating square lattice limits are given by Fig.10 and Fig.15. Note that the finite hopping amplitudes can stabilize the staggered flux phase that has circulating orbital currents (orbital antiferromagnetic state) while the extremely large hopping amplitude eventually leads to the uniform phase. It is clear from these phase diagrams that the four-particle exchange processes favor the dimerized (these are ‘partially’ dimerized) phases or the inhomogeneous orbital antiferromagnetic state (box phase) over the homogeneous orbital antiferromagnetic state (staggered flux phase). This trend persists even in the conventional ring exchange limit  $K = \lambda$  as can be seen from Fig.16 and Fig.17. Thus we conclude that the ring exchange or the four-particle exchange in general suppresses the staggered flux phase (homogeneous orbital antiferromagnetism), and instead favors the dimerized phases and/or the inhomogeneous orbital antiferromagnetic state depending on the value of  $K$ .

We note that a recent quantum Monte Carlo study [7] of a quantum XY model with a ring exchange process discovered a striped bond-plaquette ordered state at intermediate values of the ratio between the four-spin ring exchange and the nearest-neighbor Heisenberg exchange couplings. These results seem to be qualitatively consistent with our findings in the  $t$ - $J$ - $K$  model studied here even though there are obvious differences in two models. The existence of more exotic phases [4,5] like fractionalized phases in different parameter regimes of the  $t$ - $J$ - $K$  model would be an interesting subject of future study.

## ACKNOWLEDGMENTS

This work was supported by the NSERC of Canada, Canada Research Chair program of the NSERC, Canadian Institute for Advanced Research (H.Y.K. and Y.B.K.), and Alfred P. Sloan Fellowship (Y.B.K.).

- 
- [1] A. H. MacDonald, S. M. Girvin, and D. Yoshioka, Phys. Rev. B **37**, 9753 (1988).
  - [2] M. Roger, J. H. Hetherington, and J. M. Delrieu, Rev. Mod. Phys. **55**, 1 (1983).
  - [3] K. Voelker and S. Chakravarty, Phys. Rev. B **64**, 235125 (2001).
  - [4] L. Balents, M. P. A. Fisher, and S. M. Girvin, cond-mat/0110005.
  - [5] T. Senthil and O. Motrunich, cond-mat/0201320.
  - [6] A. Paramekanti, L. Balents, and M. P. A. Fisher, cond-mat/0203171.
  - [7] A. W. Sandvik, S. Daul, R. P. Singh, and D. J. Scalapino, cond-mat/0205270.
  - [8] S. Chakravarty, R. B. Laughlin, D. K. Morr, and C. Nayak, Phys. Rev. B **63**, 094503 (2001); S. Chakravarty and H. Y. Kee, Phys. Rev. B **61**, 14821 (2000); S. Chakravarty, H. Y. Kee, and C. Nayak, Int. J. Mod. Phys. B **15**, 2901 (2001).
  - [9] X. G. Wen and P. A. Lee, Phys. Rev. Lett. **76**, 503 (1996); P. A. Lee and X. G. Wen, Phys. Rev. B **63**, 224517 (2001); D. A. Ivanov, P. A. Lee, and X. G. Wen, Phys. Rev. Lett. **84**, 3958 (2000); J. Kishine, P. A. Lee, and X. G. Wen, Phys. Rev. Lett. **86**, 5365 (2001); Phys. Rev. B **65**, 064526 (2002).
  - [10] C. M. Varma, Phys. Rev. B **55**, 14554 (1997); Phys. Rev. Lett. **83**, 3538 (1999); Phys. Rev. B **61**, R3804 (2000); M. E. Simon and C. M. Varma, cond-mat/0201306.
  - [11] J. B. Marston and I. Affleck, Phys. Rev. B **39**, 11538 (1989); T. C. Hsu, J. B. Marston, and I. Affleck Phys. Rev. B **43**, 2866 (1991).
  - [12] S. Chakravarty, C. Nayak, S. Tewari, and X. Yang, cond-mat/0201228; S. Chakravarty, H. Y. Kee, and C. Nayak, cond-mat/0112109.
  - [13] P. A. Lee, cond-mat/0210113; P. A. Lee and G. Sha, cond-mat/0209572.
  - [14] C. Nayak and E. Pivovarov, cond-mat/0203580.

- [15] U.Schollwoeck, Sudip Chakravarty, J. O. Fjaerestad, J. B. Marston, and M. Troyer, cond-mat/0209444; J. B. Marston, J. O. Fjaerestad and Asle Sudbo, Phys. Rev. Lett. **89**, 056404 (2002); J. O. Fjaerestad and J. B. Marston Phys. Rev. B **65**, 125106 (2002).
- [16] R. Coldea et al., Phys. Rev. Lett. **86**, 5377 (2001); M. Matsuda, K. Katsumata, R. S. Eccleston, S. Brehmer, and H.-J. Mikeska, Phys. Rev. B **62**, 8903 (2000).
- [17] Hae-Young Kee and Yong Baek Kim, Phys. Rev. B **66**, 012505 (2002).
- [18] K. Utsumi and T. Izuyama, Prog. Theo. Phys. **58**, 1 (1977).
- [19] N. Read and S. Sachdev, Phys. Rev. Lett. **66**, 1773 (1991); S. Sachdev and N. Read, Int. J. Mod. Phys. **B5**, 219 (1991).
- [20] C. H. Chung, J. B. Marston and R. H. McKenzie, J. Phys. Cond. Matt. **13**, 5159 (2001).
- [21] M. Vojta, Y. Zhang, and S. Sachdev, Phys. Rev. B **62**, 6721 (2000).
- [22] William H. Press, Saul A. Teukolsky, William T. Vetterling, and Brian P. Flannery 1992 *Numerical Recipes in C: The Art of Scientific Computing, Second Edition*, pp. 451 – 455 (Cambridge University Press, New York, NY).
- [23] T. Dombre and G. Kotliar Phys. Rev. B **38**, 855 (1989).
- [24] C. H. Chung, J. B. Marston and S. Sachdev Phys. Rev. B **64**, 134407 (2001).
- [25] J. B. Marston, Phys. Rev. Lett. **64**, 1166 (1992); D. H. Kim and P. A. Lee, Annals. Phys. **272**, 130 (1999).